Spectral-hole-burning study of the hyperfine interaction in axial Eu^{3+} centers in CaF_2, SrF_2, and BaF_2

A. J. Silversmith
Physics Department, Hamilton College, Clinton, New York 13323

R. M. Macfarlane
IBM Research Division, Almaden Research Center, 650 Harry Road, San Jose, California 95120-6099
(Received 18 November 1991)

Hole-burning spectra of Eu^{3+} transitions in axial centers of alkaline-earth fluorides are presented. These spectra, along with optically detected nuclear-magnetic-resonance results, are used to analyze the hyperfine interactions in the $^7F_0$ ground state and in the $^5D_0$ optically excited state. The axial nature of these centers simplifed the theoretical analysis from which we obtained the nuclear-quadrupole-interaction strength and the nuclear-magnetic moment quenching factor. An improved value of the ratio of the quadrupole moments of ^{153}Eu and ^{151}Eu of 2.553 ± 0.001 is also given.

I. INTRODUCTION

Spectral hole burning and optically detected nuclear-magnetic-resonance (ODNMR) are two high-resolution laser spectroscopic techniques that have proven to be very useful in the study of hyperfine coupling in trivalent europium centers in crystals. In recent years several publications have reported studies of the hyperfine coupling, in zero field as well as in the presence of an external magnetic field, for Eu^{3+} centers in various host materials. The basic theoretical framework for analysis of the hyperfine interaction in the ground state of $Eu^{3+}(^7F_0)$ was laid out in a 1957 paper by Elliott.[1] He calculated the hyperfine, magnetic, and quadrupole interactions up to second order. Two major conclusions arise from this work. First, there is a substantial quenching of the ground-state nuclear moment due to a magnetic interaction with the low-lying $^7F_1$ multiplet. This makes conventional NMR experiments on Eu^{3+} systems very difficult, and indeed, before the advent of high-resolution laser techniques, there were few experimental data available on hyperfine coupling in europium. Elliott's second theoretical prediction follows from a calculation of various contributions to the electric-field gradient (EFG) at the Eu nucleus, which couples with the quadrupole moment of the nucleus to determine the zero-field hyperfine structure. He concluded that the major contribution to the EFG was a second-order effect of the polarization of the $4f$ electrons, and that the EFG set up by the lattice itself was a much smaller contributing factor. This work was modified some years later by Judd, Lovejoy, and Shirley,[2] who realized that the core electrons amplify the lattice EFG, and this antishielding effect makes the lattice contribution important as well. Subsequent work by Edmonds[3] and Blok and Shirley[4] discussed the quadrupole and shielding effects in Eu^{3+} within the framework of shielding phenomena in rare-earth ions in general. The recent experimental work on Eu^{3+} centers has shown that Elliott's original theoretical predictions with these modifications (summarized in Sec. III), can provide a good description of the hyperfine coupling in the $^7F_0$ and $^5D_0$ states of Eu^{3+}.

To confront the theory, experimental studies on optical centers of axial symmetry are highly desirable since the nuclear quadrupole and electronic (crystal field) z axes are coincident, and the critical parameters of the theory are more readily determined. For example, in the axial case, the general tensorial calculations are reduced to scalar calculations involving the diagonal components. Much of the work published on hyperfine coupling in Eu^{3+} centers has dealt with lower symmetry centers.[5–8] It is the goal of this work to demonstrate experimentally that a complete and consistent agreement with the theoretical treatments can be obtained using axial centers of C_{4v} symmetry in CaF_2, SrF_2, and BaF_2.

There are three hole-burning studies of hyperfine coupling in axial Eu^{3+} centers in the literature: $LiYF_4:^{3+}$,[9] $CaF_2:Eu^{3+}:O^{2-}$,[10] and $CdF_2:Eu^{3+}:O^{2-}$,[10] but all of these

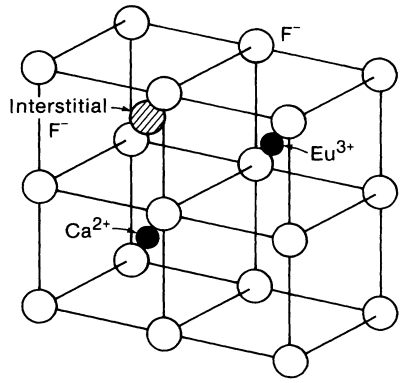

FIG. 1. The local environment of the Eu^{3+} ion. Charge compensation is due to a F^- in the nearest vacant body center position in the ⟨100⟩ direction. The resulting symmetry is C_{4v}, and the ⟨100⟩ direction forms the z axis.

TABLE I. Spectroscopic information for the C_{4v} centers in Eu^{3+}, SrF_2, and BaF_2.

	CaF_2	SrF_2	BaF_2
$^5D_0$ energy (cm^{-1})	17 283.5	17 295.6	17 302.0
$^7F_0 \rightarrow {}^5D_0$ linewidth (FWHM, GHz)	1.8	1.3	2.3
$^7F_1$ energies (cm^{-1}): A_2	450	431	395
E	303	325	328
$^7F_1$ splitting (cm^{-1})	147	106	67

systems have characteristics which prevent a complete and satisfactory analysis. In $LiYF_4:Eu^{3+}$, a center of S_4 symmetry, the $^7F_0 \rightarrow {}^5D_0$ transition is only magnetic dipole allowed and is very weak. As a result, a hole-burning spectrum could not be generated. All of the experimental results are from ODNMR, and pertain only to the $^7F_0$ ground state; no information about the hyperfine structure in the $^5D_0$ state is available, so a complete analysis was not possible. In addition, difficulties were encountered in obtaining consistent magnetic-moment quenching parameters in the ground state. The magnitudes of the effective magnetic moments in the xy plane and along the z axis give inconsistent determinations of $\langle r^{-3} \rangle$, the average inverse cube distance of the $4f$ electrons from the nucleus, and this discrepancy is still not resolved. The oxygen compensated centers in CaF_2 and CdF_2 are composed of a substitutional Eu^{3+} ion in a Ca (Cd) site, charge compensated by an O^{2-} ion in the nearest fluorine site in the $\langle 111 \rangle$ direction; the resulting local symmetry is C_{3v}. The two centers have anomalous spectroscopic behavior.[11-13] Very large crystal-field-induced splittings and a high $^7F_0 \rightleftharpoons {}^5D_0$ oscillator strength indicate that these centers are not typical rare-earth centers where crystal-field effects are a small perturbation to the free ion character. In addition, $^5D_J \rightarrow {}^7F_1(A_2)$ emission is not observed, and thus the positions of the $^7F_1(A_2)$ level in both centers, necessary for evaluation of Hamiltonian terms describing hyperfine interactions in the $^7F_0$ ground state, are not known. The hyperfine structure in these centers could not be explained using the theoretical approach of Refs. 1–4, where relevant matrix elements were calculated using the free ion wave functions. To achieve a consistent description, it was necessary to introduce matrix elements which deviated from the free ion values by as much as 60%.[10]

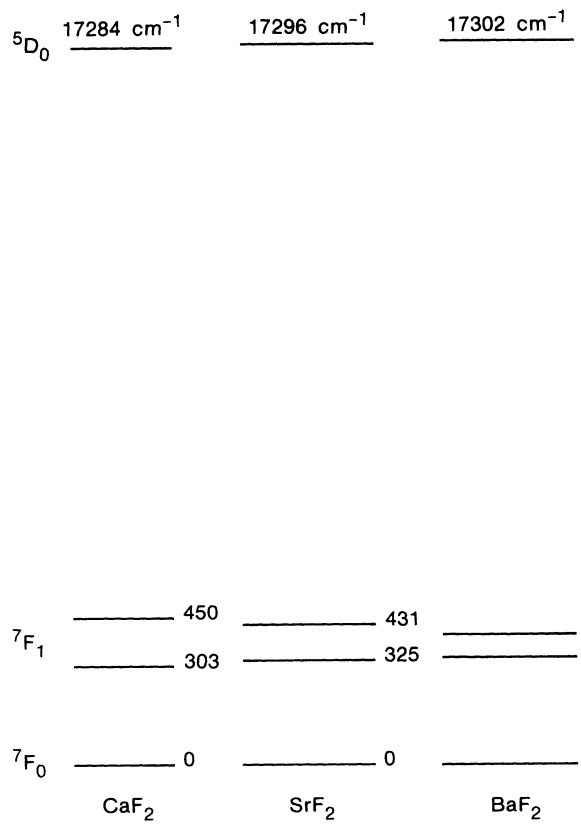

FIG. 2. Positions of the energy levels $^7F_0$, $^7F_1$, and $^5D_0$ for CaF_2, SrF_2, and BaF_2.

The tetragonal centers on which we report here are much more amenable to a complete understanding of the $^7F_0$ and $^5D_0$ hyperfine coupling. The energies of $^7F_1$ and $^5D_1$ crystal-field levels, which are needed for evaluation of magnetic effects, are readily determined. Well-resolved hole-burning spectra, in combination with ODNMR, allow a complete determination of the zero-field hyperfine structure in both electronic states. The centers are composed of a substitutional Eu^{3+} in a Ca^{2+} (or Sr^{2+} or Ba^{2+}) site, charge compensated by an interstitial F^- in one of the neighboring vacant body center positions in the lattice, as seen in Fig. 1. The resulting site symmetry is C_{4v}, with the z axis of the site along a $\langle 100 \rangle$ crystal axis. The positions of some of the energy levels in the CaF_2 (Ref. 14) and SrF_2 (Ref. 15) centers has previously been reported; we have verified these results and performed additional experiments to determine the positions of the energy levels relevant to our discussion (Table I and Fig. 2). The centers have small crystal-field splittings typical for Eu^{3+} systems, and there are no apparent anomalies in the spectra. These are the first hole-burning spectra published for an axial Eu^{3+} system, and the structure has shed considerable light upon the hole-burning mechanism in sites of axial symmetry.

II. EXPERIMENTAL TECHNIQUES

All experiments were performed at 1.8 K on single crystals doped with ~0.01% Eu^{3+}. Spectral holes were

burned by exposing the sample to the unattenuated laser beam (~50 mW) from a narrow-band (1-MHz jitter linewidth) dye laser, with the frequency tuned within the inhomogeneously broadened absorption line, usually near the center of the line in order to generate hole-burning spectra on a fairly flat background. The $^5D_0 \rightarrow {}^7F_2$ red emission near 610 nm was monitored and was seen to drop quickly to a saturated level (near zero in these centers) due to redistribution of population among the hyperfine levels in the ground electronic state.[5,16] This condition of redistributed population lasts several hours in these samples if the crystal is maintained at helium temperature. The resulting hole-burning spectrum was then recorded by attenuating the laser by about a factor of 100, and scanning the laser in frequency around the original burn frequency while monitoring $^5D_0 \rightarrow {}^7F_2$ fluorescence.

The optical pumping phenomenon, which produces a nonequilibrium distribution of population among the ground-state hyperfine components, is also exploited in an ODNMR experiment. The laser is kept at fixed frequency, maintaining hole burning, while radio-frequency (rf) radiation is simultaneously applied to the sample.[17] The rf is scanned in frequency while the fluorescence from the $^5D_0$ level is again monitored. When the rf becomes resonant with a ground-state hyperfine splitting, transitions which cause hole filling are stimulated, and the laser interacts with an increased number of ions. The result is a temporarily increased fluorescence level. When the rf is scanned past the resonance, hole burning causes the emission level to decrease again to the saturated level. Ground-state hyperfine splittings can be read directly from the positions of hole-filling signals in the ODNMR spectrum.

III. ZERO-FILLED HYPERFINE COUPLING

A. Theory

We summarize the theory of the hyperfine coupling in the $Eu^{3+}({}^7F_0)$ ground state based on the model originally proposed by Elliott[1] and extended and applied by other workers.[5,7,9,10,12]

In the absence of a magnetic field, the spin Hamiltonian for the hyperfine coupling in either the $^7F_0$ ground state $|g\rangle$ or the $^5D_0$ optically excited state $|e\rangle$, of Eu^{3+} in an axial state has the form

$$H = P^{g,e}(I_z^2 - \tfrac{1}{3}I^2) , \tag{1}$$

where I is the nuclear spin operator, and $P^{g,e}$ the quadrupole coupling parameter in the ground or excited states. Unless specifically required in what follows, the superscripts g and e will be omitted. P can be written

$$P = P_{\text{latt}} + P_{4f} + P_{pq} , \tag{2}$$

where P_{latt} and P_{4f} are the quadrupole coupling parameters for the lattice and $4f$ contributions to the electric-field gradient mentioned briefly in the Introduction, and P_{pq} is the pseudoquadrupole term. Expressions for them are as follows:

$$P_{\text{latt}} = \frac{-3Q}{I(2I-1)}(1-\gamma_\infty)A_2^0 , \tag{3}$$

$$P_{4f} = \frac{6e^2Q}{I(2I-1)}\frac{A_2^0\langle r^2\rangle(1-\sigma_2)}{\Delta_2} . \tag{4}$$

Q is the quadrupole moment, I is the nuclear spin, A_2^0 is the crystal-field parameter, $\langle r^2\rangle$ is the mean-square distance between the $4f$ electrons and the nucleus, Δ_2 is the energy of the ${}^7F_2(A_2)$ level, and $(1-\gamma)_\infty$ and $(1-\sigma_2)$ are shielding parameters, introduced in Ref. 4 and reviewed in Ref. 12. The pseudoquadrupole coupling parameter P_{pq} is due to a second-order magnetic hyperfine interaction between $J=0$ states and nearby $^7F_1$ (or $^5D_1$):

$$P_{pq} = A_J^2[\tfrac{1}{2}(\Lambda_{xx}+\Lambda_{yy})-\Lambda_{zz}] , \tag{5}$$

where

$$\Lambda_{\alpha\alpha} = \sum_{n=1}^{2J+1}\frac{\langle 0|J_\alpha|1\rangle\langle 1|J_\alpha|0\rangle}{\Delta E_{1,0}} \tag{6}$$

with $|0\rangle$ representing $^7F_0$ or $^5D_0$ and $|1\rangle$ representing $^7F_1$ or $^5D_1$. In the $^7F_0$ state, P_{pq} is a few percent of the total P; in the $^5D_0$ state it is even smaller. In fact, in our experiments, the energy shift due to the pseudoquadrupole coupling in the $^5D_0$ level is not measurable.

Europium has a nuclear spin of $\frac{5}{2}$ and the quadrupole spin-Hamiltonian term (1) yields three energy levels, all doubly degenerate, as shown schematically in Fig. 3. The overall magnitude of the hyperfine splitting is proportional to P. The axial nature of these centers serves to simplify the problem in two ways. First, the spin Hamiltonian (1) has no terms involving I_x and I_y, as would be the case in lower symmetry. The hyperfine states are then pure I_z quantum states. Second, P_{latt} and P_{4f} combine in a simple way—P is the arithmetic sum of the two contributions. (In this work, the small pseudoquadrupole parameter P_{pq} is not analyzed in detail, but it too is added in the same way.) In lower symmetry centers, P_{latt} and P_{4f} are

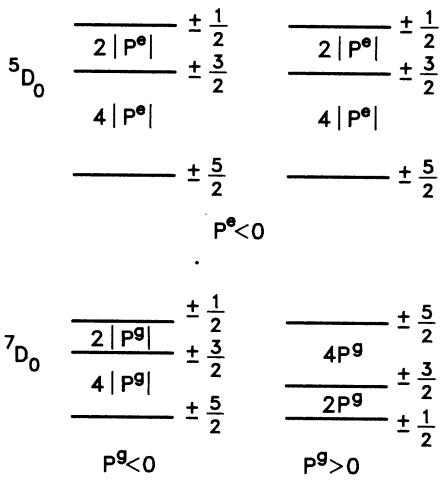

FIG. 3. Schematic representation of the zero-field hyperfine structure in the ground and excited states.

tensor quantities, whose principal axes do not coincide, and analyzing their combined effect is a more complicated problem.[7]

Some general remarks can be made about the different character of the hyperfine coupling in the two electronic states by making rough calculations of the relative signs and magnitudes of P_{4f} and P_{latt} in the two states. For both of these spherically symmetric ($J=0$) states, the $4f$ electrons do not contribute to the EFG in first order. However, a second-order contribution exists due to coupling via the crystal field with the nearby $^7F_2$ or $^5D_2$ levels of appropriate symmetry, resulting in a nonzero P_{4f}. P_{latt} is identical for the $^7F_0$ and $^5D_0$ levels, as it is a result of the static crystal-field environment of the ion, but P_{4f} is very different for the two electronic states. It is much larger for the $^7F_0$ level than for the $^5D_0$ level because the $^7F_2$ levels are about 1000 cm^{-1} above $^7F_0$, while the $^5D_0$-$^5D_2$ energy spacing is 4000 cm^{-1}. [These energies are Δ_2 in the denominator of (4).] The two contributions P_{latt} and P_{4f} have opposite signs and thus a significant cancellation effect occurs in the $^7F_0$ state where they are of comparable magnitude. In the $^5D_0$ level, P_{4f} is much smaller than P_{latt}, and thus P is roughly equal to P_{latt}. So, as a general rule, the $^7F_0$ hyperfine splittings (proportional to P_g) are smaller than those in the $^5D_0$ state; this is indeed what is measured in Eu^{3+} systems.

In europium, there are two naturally occurring isotopes of nearly equal abundance, ^{151}Eu and ^{153}Eu, both with spin $\frac{5}{2}$. They have different quadrupole moments, and therefore different hyperfine structures. P_{latt} and P_{4f} are directly proportional to the quadrupole moment of the nucleus, and if it were not for the presence of P_{pq}, the ratio of the hyperfine splittings in ^{153}Eu to those in ^{151}Eu would be exactly equal to the ratio of the quadrupole moments. The deviation from this ratio for the measured splittings gives a measure of the importance of the pseudoquadrupole interaction, which, as we have stated, is negligible in the $^5D_0$ state.

B. Experimental results

Figure 4 shows zero-field hole-burning spectra of Eu^{3+} in the C_{4v} centers in CaF_2, SrF_2, and BaF_2. A pattern of only three antiholes per isotope on either side of the central hole is recorded. This is markedly different from hole-burning spectra of Eu^{3+} centers of lower symmetry, where strong side holes and more antihole structure have always been present.[5,6,8] As we explain next, it is this difference which has allowed us to develop a new understanding of the hole-burning process in axial Eu^{3+} centers.

The hole-burning process in Eu^{3+} may be thought of as being composed of two steps: (i) an ion absorbs a photon and makes a transition from the $^7F_0$ to the $^5D_0$ state, and (ii) the ion relaxes back to the ground electronic state through a series of radiative and nonradiative steps. These two steps must result in the ion ending up in a different hyperfine level, i.e., its I_z quantum number having changed. Scanning the hole and recording the associated hole-burning spectrum involves a third process: the ion again absorbs a photon, is excited to the $^5D_0$ state, and contributes to the observed emission level, which is monitored as a measure of the laser absorption.

In axial centers, like those under discussion, I_z is a good quantum number, and ideally, optical absorption and emission between the $^7F_0$ and $^5D_0$ states should occur only for $\Delta I_z=0$ transitions. According to this reasoning, no hole burning should ever occur. Ions in a given I_z spin state should remain in that state throughout the optical cycling, and the population redistribution hole-burning mechanism should not be possible. However, hole burning *is* observed, and the hole-burning spec-

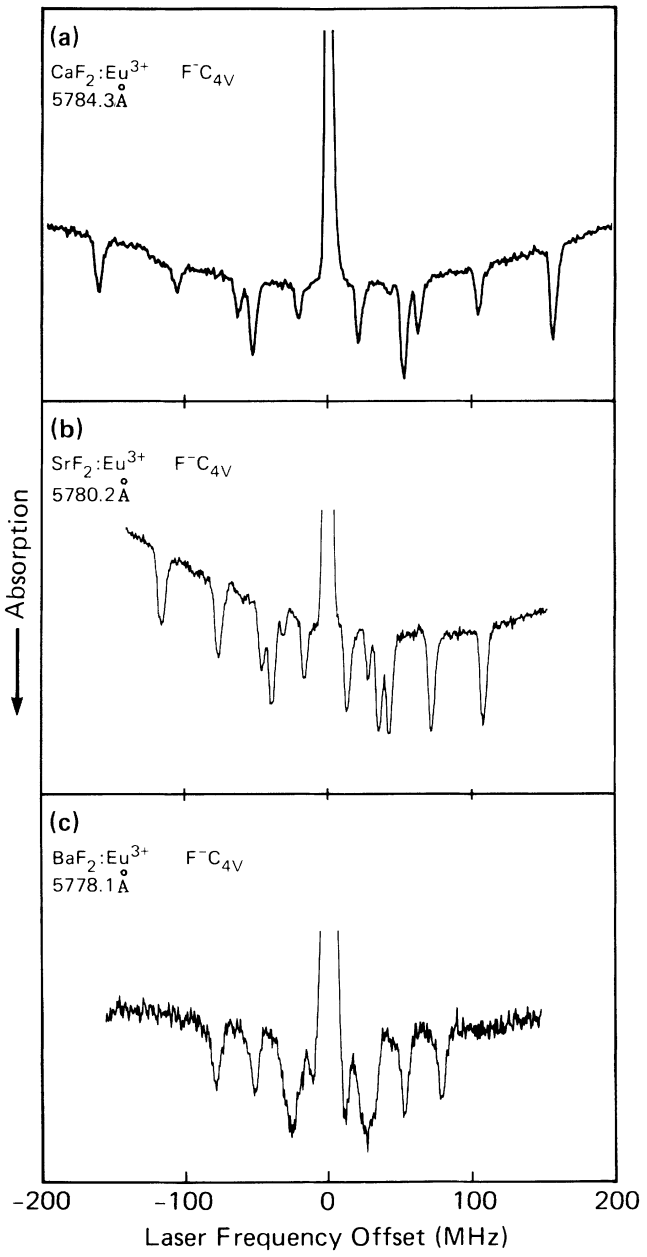

FIG. 4. Zero-field hole-burning spectra of the $^7F_0 \rightarrow {}^5D_0$ transition of Eu^{3+} in (a) CaF_2, (b) SrF_2, and (c) BaF_2.

trum, as well as the presence of ODNMR signals, proves that population redistribution among hyperfine levels is the correct mechanism. Therefore, the $\Delta I_z=0$ selection rule appears not to be strictly obeyed. If this selection rule is relaxed slightly, and the $\Delta I_z\neq 0$ paths for both absorption and relaxation are allowed with some small and comparable probability, then the resulting hole-burning spectrum arises as follows. Auxiliary holes are placed symmetrically on either side of the central hole, displaced by frequencies equal to excited-stated ($^5D_0$) hyperfine splittings. Also present are antiholes, found at frequencies corresponding to sums or differences of ground- and excited-state hyperfine splittings, and symmetrically placed about the central hole. Sums are observed when $P(^5D_0)$ and $P(^7F_0)$ are of opposite signs; differences are observed when they are of the same sign. Lastly, additional symmetrically placed antiholes are found at frequencies corresponding to ground-state hyperfine splittings. This sort of spectrum has been reported for several Eu^{3+} centers of low symmetry,[5,8] but is clearly not what is observed here.

Table II lists the positions of the antiholes due to each isotope, measured with respect to the central hole, and determined from the hole-burning spectra. The observed antiholes are identified with the appropriate isotope; this isotope labeling can be done readily because hyperfine structure in ^{153}Eu is larger than that in ^{151}Eu by a factor of approximately $^{153}Q/^{151}Q$. The ground-state hyperfine splittings were derived simply and directly from ODNMR spectra, examples of which are given in Fig. 5. (Results are also summarized in Table II.) The $^7F_0$ hyperfine splittings do *not* match the positions of the observed antiholes. The observed antihole frequencies are therefore assigned to sums or differences of ground- and excited-state hyperfine splittings. The antihole frequencies are in the ratio 1:2:3 and, for the moment, we label them $\pm 2(P^g-P^e)$, $\pm 4(P^g-P^e)$, and $\pm 6(P^g-P^e)$, where P^g and P^e are the quadrupole parameters in the ground and excited states, defined in Fig. 3. The $\pm$ outside the parentheses indicates that the spectral features are found symmetrically placed on either side of the central hole. The quadrupole parameters P^g and P^e may be positive or negative so their relative signs are important in these expressions.

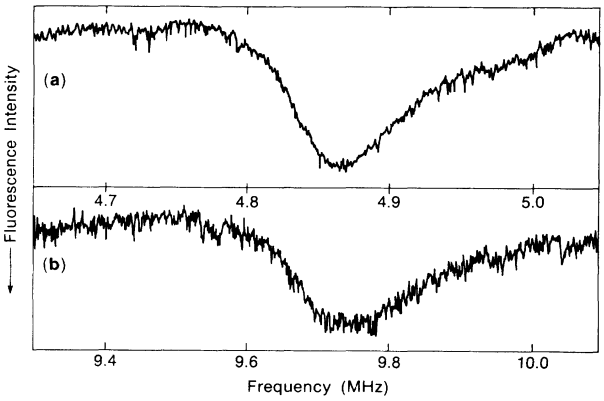

FIG. 5. ODNMR signal corresponding to (a) the $|\pm\frac{1}{2}\rangle \Longleftrightarrow |\pm\frac{3}{2}\rangle$ transition and (b) the $|\pm\frac{3}{2}\rangle \Longleftrightarrow |\pm\frac{5}{2}\rangle$ transition between ground-state hyperfine levels in the CaF_2 center.

Generation of zero-field hole-burning spectra, which contain no sideholes and no antiholes at ground-state hyperfine frequencies, can occur in the following way. A small but nonzero probability for a $\Delta I_z\neq 0$ transition is introduced *during the relaxation process only.* That is, an ion may undergo a change in I_z quantum number while in $^5D_0$, or during the relaxation route back to the ground state. The absorption ($^7F_0\rightarrow{}^5D_0$) transitions must be governed by a strict $\Delta I_z=0$ selection rule. If one predicts the features that will appear in a hole-burning spectrum, following these rules, the agreement is perfect. The only spectral features that appear in the spectra in Fig. 4 are antiholes that are found at frequencies corresponding to sums or differences of ground- and excited-state hyperfine splittings. It is not possible to determine where the change in I_z happens; the $^5D_0$ lifetime is longer than that

TABLE II. Positions of features in hole-burning and ODNMR spectra, for both isotopes of europium. A blank space indicates that the spectral feature was not visible or could not be clearly resolved.

	CaF_2		SrF_2		BaF_2	
	^{151}Eu	^{153}Eu	^{151}Eu	^{153}Eu	^{151}Eu	^{153}Eu
Positions (MHz) of zero-field antiholes	±21.9 ±42.7 ±63.7	±53.2 ±106.3 ±160	±14.8 ±29.6 ±44.1	±36.7 ±73.4 ±110	±11 ±21 ±30	±26 ±50 ±75
Positions (MHZ) of field-induced auxiliary holes	±26		±3 ±25	±31 ±63	−9 −16	−41
Positions (MHz) of field-induced antiholes	±5 ±10	±14 (weak)	±5	±5		
Ground-state ODNMR signals (MHz)	4.83 9.67	13.2 26.4	1.78 3.56		1.95 3.9	5.37 10.75

of any ^7F_J states, which the ion may encounter on its return to the ground state, so it is perhaps more likely that the "spin flip" occurs in the $^5D_0$. Because the antiholes at $\pm 6(P^g - P^e)$ are of comparable intensity to those at the lower frequency separations, we see that a $\Delta I_z = \pm 2$ transition is of comparable probability to a $\Delta I_z = \pm 1$.

A second experiment supported this reasoning. Application of a weak magnetic field (~ 0.5 kG) perpendicular to the local z axis served to force the center to lose its purely axial symmetry. The magnetic field mixed the nuclear spin states slightly which resulted in a small probability for optical transitions which were forbidden in zero field. (In these cubic crystals there are "local z axes" in three orthogonal directions; polarization of the excitation laser along a $\langle 100 \rangle$ crystal axis selected centers with a common and unique local z axis.) Figures 6 and 7 show the new spectra which were generated in this way for CaF_2:Eu^{3+} and SrF_2:Eu^{3+}, respectively. They contain the more complicated structure, comprised of side holes and antiholes, described above. In this case, the "$\Delta I_z \neq 0$" transitions occur with some probability in all three steps. The field was kept weak enough so that the splittings of I_z states which were doubly degenerate in zero field is much smaller than 2 MHz, the laser linewidth determined resolution in the hole-burning spectrum, so there was no observable broadening or splitting of the spectral features.

Conveniently, the new spectral features in the nonaxial spectrum allow complete determination of the hyperfine structure in both electronic states, and also a determination of the relative signs of P in the two electronic states. The ground-state ($^7F_0$) quadrupole splittings were determined by ODNMR. The auxiliary holes in the nonaxial spectra are found at frequencies corresponding to $^5D_0$ quadrupole splittings. With these hyperfine splittings determined, it is a simple matter to decipher the remaining spectral features, and, in particular, to label the antihole positions in the original spectra (Fig. 4) as sums or differences of excited- and ground-state splittings. This accomplished, the relative sign of $P(^5D_0)$ and $P(^7F_0)$ can be determined. Results of this analysis are summarized in Table III.

With the magnitudes of $P(^5D_0)$ and $P(^7F_0)$ determined, as well as their relative signs, some information

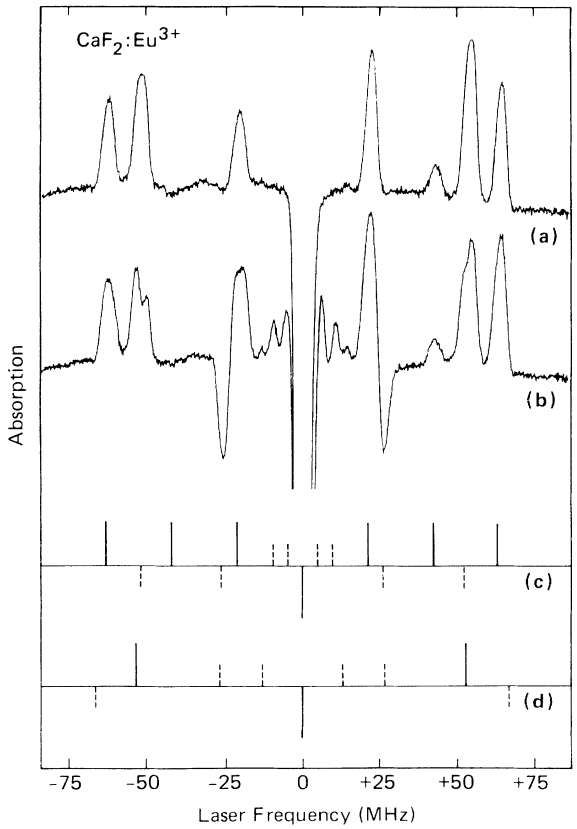

FIG. 6. Hole burning in the presence of a magnetic field for CaF_2:Eu^{3+} at 5784.3 Å. (a) Zero-field spectrum. (b) Hole burning and probing done in the presence of $H \approx 0.5$ kG, perpendicular to local z axis. (c) Spectral features assigned to ^{151}Eu. Solid lines are those present in zero-field spectrum; dashed lines represent extra holes and antiholes which are found in (b). (d) Features assigned to ^{153}Eu.

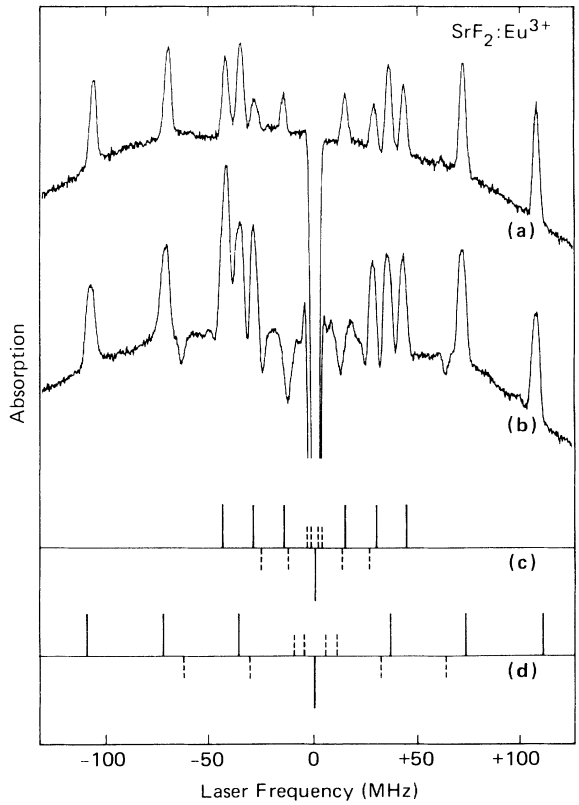

FIG. 7. Hole burning in the presence of a magnetic field for SrF_2:Eu^{3+} at 5780.2 Å. (a) Zero-field spectrum. (b) Hole burning and probing done in the presence of $H \approx 0.5$ kG, perpendicular to local z axis. (c) Spectral features assigned to ^{151}Eu. Solid lines are those present in zero-field spectrum; dashed lines represent extra holes and anthiholes which are found in (b). (d) Features assigned to ^{153}Eu.

TABLE III. Parameters describing the nuclear magnetic moment and the quadrupole interaction. The first two rows pertain to the nuclear-magnetic-moment quenching parameter. It was not possible to obtain measured values for the SrF_2 and BaF_2 centers because only very dilute samples were available, and the ODNMR spectra had insufficient signal-to-noise ratio to allow determination of the α parameters. Hyperfine parameters were determined from the experimental results in Table II.

	CaF_2 ^{151}Eu ^{153}Eu	SrF_2 ^{151}Eu ^{153}Eu	BaF_2 ^{151}Eu ^{153}Eu
$\alpha_{xy}(^7F_0)$[a]	0.98(0.96)	(0.89)	(0.88)
$\alpha_z(^7F_0)$[a]	0.56(0.64)	(0.67)	(0.73)
Relative sign of $P(^5D_0)$ and $P(^7F_0)$	same	opposite	opposite
Sign of $P(^7F_0)$	negative	positive	positive
P_{latt} (MHz)	−13	−6.5	−4.5
P_{4f}(MHz)	+11	+7.4	+5.5

[a]Calculated values given in parentheses.

can be derived in a straightforward way about P_{latt} and P_{4f}, $P(^5D_0)$ is approximately equal to P_{latt}, whose magnitude is proportional to A_{20}, but which has the opposite sign.[4] The sign of A_{20} is readily determined from the order of the E and A levels in the $^7F_1$ multiplet.[1] For these centers, A_{20} is positive, so P_{latt} is negative.

Therefore, $P(^5D_0)$ is negative in all three centers, and the last row of Table III implies that $P(^7F_0)<0$ in CaF_2 and $P(^7F_0)>0$ in SrF_2 and BaF_2. In the latter two sites, the magnitude of P_{4f} is greater than the magnitude of P_{latt}, whereas in CaF_2, P_{4f} is smaller in magnitude than P_{latt}, and only partial cancellation takes place. The last two lines in Table III give approximate values of P_{latt} and P_{4f}; the pseudoquadrupole coupling has been neglected, and $P(^5D_0)\approx P_{\text{latt}}$ for these calculations.

The A_2 and E level spacing in the $^7F_1$ multiplet is also roughly proportional to A_{20}, so a semiquantitative comparison can be made between the relative values of P_{latt} and the $^7F_1$ crystal-field splitting in the three materials. For CaF_2, SrF_2, and BaF_2, the $^7F_1$ splittings are 147, 106, and 67 cm^{-1}, respectively, in the ratio of 2.2:1.6:1.0. The P_{latt} values are in the ratio of 2.1:1.3:1.0.

Pseudoquadrupole coupling [see Eqs. (5) and (6)] makes a small measurable contribution to the zero-field hyperfine coupling in the $^7F_0$ ground state. The clearly observable effect is seen by calculating the ratio of $P(^7F_0)$ for the two isotopes ^{153}Eu and ^{151}Eu. If there were no pseudoquadrupole effect, this ratio would equal the ratio of the nuclear moments. This value of $^{153}Q/^{151}Q$ was in fact determined as 2.556 ± 0.005 by measuring the ratio of hyperfine splittings in the $^5D_0$ state of another axial system, CaF_2:Eu^{3+}:O^{2-}, which more readily exhibits excited-state ODNMR signals.[17] We have repeated these measurements and find an improved value of 2.553 ± 0.001, which is consistent with their measurement. In the C_{4v} systems under discussion here, the ratio $^{153}P(^7F_0)/^{151}P(^7F_0)$ differs markedly from 2.553, which is an indication of the presence of the pseudoquadrupole effect. In CaF_2 the ratio is 2.73, and in BaF_2 it is 2.75.

Substitution of numerical values of A_J and the $\langle 0|J_\alpha|1\rangle$ matrix elements into Eqs. (5) and (6) yields the result

$$P_{pq}=85\left[\frac{1}{\Delta E_{O,E}}-\frac{1}{\Delta E_{O,A}}\right]\text{ MHz} . \tag{7}$$

If the energy gaps (ΔE's) are in cm^{-1} for CaF_2 and BaF_2, then the calculated values of P_{pq} are 0.092 and 0.044 MHz, respectively. Taking this effect into account should enable us to "correct" the observed $^{153}P/^{151}P$ ratios to yield the $^{153}Q/^{151}Q$ ratio of 2.553. This, however, does not work. In CaF_2, the pseudoquadrupole correction gives a quadrupole moment ratio of 2.64. In BaF_2, because the sign of the overall P is *opposite* to that in CaF_2, but P_{pq} has the *same* sign, the "correction" actually takes the ratio in the wrong direction, from 2.75 to 2.91. This inconsistency is not understood at the present time.

IV. QUENCHED NUCLEAR MAGNETIC MOMENTS

A. Theory

Another effect which Elliott predicted[1] is the quenching of the nuclear magnetic moment in the ground ($^7F_0$) state. He showed that the effective Zeeman Hamiltonian can be written in the form

$$H'=\frac{\mu_N\beta_N}{I}(1-\alpha)\bar{B} , \tag{8}$$

where

$$\alpha=\frac{20}{3}\frac{\langle 0|(L+2S)|1\rangle\langle r^{-3}\rangle}{\Delta_i} . \tag{9}$$

Δ_i is the energy separation between the $J=0$ and 1 levels of appropriate symmetry to couple with a field component in the ith direction. The effective magnetic moment is $\mu_{\text{eff},i}=(1-\alpha_i)\mu_N$, where μ_N is the bare europium magnetic moment. When an external magnetic field is applied, the doubly degenerate I_z states split, and the size

of the field-induced splitting is determined by μ_{eff}, not the bare moment μ_N. The matrix element $\langle 0|(\mathbf{L}+2\mathbf{S})|1\rangle$ is equal to 2 between the $^7F_0$ and $^7F_1$ states, and $\sqrt{2}$ between the $^5D_0$ and $^5D_1$ states. The value of $\langle r^{-3}\rangle$ is given in Ref. 4 as 49×10^{24} cm^{-3}. In most Eu^{3+} systems, the Δ_i energy splitting is such that α comes out fairly close to 1, and the effective moment is much smaller than the bare moment μ_N; thus the term "quenching" of the magnetic moment.

B. Experimental implications

The quenching of the nuclear magnetic moment manifests itself in several ways here. Referring to Figs. 6 and 7, it can be seen that with magnetic fields of equal magnitude, extra spectral features appear more obviously in SrF_2 than in CaF_2. Apparently, the SrF_2 center is made more nonaxial by the presence of a field of the same magnitude, than the site in CaF_2. This is readily understood in terms of the quenching effect of the ground-state magnetic moment. The degree of nuclear level mixing, and thus the degree of nonaxial behavior introduced, is determined by $(1-\alpha_{xy})\mu_N$, the quenched moment for fields in the xy plane, and by the zero-field quadrupole spacings. Table III contains calculated values of α_{xy} and α_z for the three centers, and measured values for CaF_2. The measurement was done by measuring the splitting of the ODNMR lines as a function of external field. A more highly doped sample was used for this measurement, and the lower concentration of Eu^{3+} in our crystals of SrF_2 and BaF_2 produced ODNMR signals having an insufficient signal-to-noise ratio. Consider the $^7F_0$ hyperfine levels first. In CaF_2, α_{xy} is calculated using Eq. (3) to be 0.96 (we measure 0.98 by measuring the splitting of ODNMR lines in an external field), and in SrF_2, α_{xy} is calculated to be 0.89. Thus the effective nuclear magnetic moment in the CaF_2 ground state is quenched considerably more than in SrF_2. The SrF_2 center has zero-field hyperfine splittings about three times smaller than the CaF_2 center. Both of these considerations lead to greater field-induced mixing of hyperfine states in $SrF_2(^7F_0)$ than $CaF_2(^7F_0)$, and thus to more nonaxial character in this experiment. Mixing of hyperfine levels in the presence of the field also occurs in the $^5D_0$ electronic state when the field is applied. In this case, the moment is essentially unquenched, but the zero-field splittings are large compared to those in $^7F_0$. Again, more mixing occurs for the SrF_2 center due to the smaller quadrupole splittings.

Similar reasoning shows that much less nonaxial behavior is expected from the ^{153}Eu isotope, because its magnetic moment is a factor of 2.2 smaller and its quadrupole splittings are a factor of about 2.5 larger than for ^{151}Eu, and both of these considerations decrease the amount of field-induced mixing. It is therefore understandable that fewer new features from ^{153}Eu appear in the spectra shown in Fig. 6. For the CaF_2 system, the magnetic field only has significant effect on the ^{151}Eu hole-burning pattern; only one very weak feature due to ^{153}Eu is visible. In the SrF_2 center, the smaller $^7F_0$ quadrupole splittings and larger effective moment result in significant wave-function mixing for both isotopes. The experiment was also performed on the BaF_2 site; only one extra feature, a side hole at -41 MHz, was clearly visible.

V. CONCLUSIONS

The hyperfine structure in the $^7F_0$ and $^5D_0$ states of Eu^{3+} has been studied in C_{4v} centers in CaF_2, SrF_2, and BaF_2. The hole-burning spectra are the first to be reported for axial Eu^{3+} centers, and their structure have allowed for some new insight into the hole burning mechanism in axial centers. Analysis of the simple zero-field hole-burning spectra, consisting of only three antiholes per isotope in addition to the central hole, showed that the $\Delta I_z\neq0$ transition, necessary for population redistribution hole burning, cannot occur during $^7F_0\rightarrow{}^5D_0$ excitation. It must take place while the ion is in the $^5D_0$, or during the ion's relaxation path back to the ground state. The axial nature of these centers has allowed a complete analysis of the lattice and $4f$-electron contributions to the quadrupole coupling.

[1] R. J. Elliott, Proc. R. Soc. London Ser. B **70**, 119 (1957).
[2] B. R. Judd, C. A. Lovejoy, and D. A. Shirley, Phys. Rev. **128**, 1733 (1961).
[3] D. T. Edmonds, Phys. Rev. Lett. **10**, 129 (1963).
[4] J. Blok and D. A. Shirley, Phys. Rev. **143**, 278 (1965).
[5] R. M. Shelby and R. M. Macfarlane, Phys. Rev. Lett. **47**, 1172 (1981).
[6] R. M. Macfarlane, R. M. Shelby, A. Z. Genack, and D. A. Weitz, Opt. Lett. **5**, 462 (1980).
[7] L. E. Erickson, Phys. Rev. B **34**, 36 (1986).
[8] A. J. Silversmith and N. B. Manson, J. Phys. C **17**, L97 (1984).
[9] K. K. Sharma and L. E. Erickson, J. Phys. C **18**, 2935 (1985).
[10] A. J. Silversmith, A. P. Radlinski, and N. B. Manson, Phys. Rev. B **34**, 7554 (1986).
[11] A. J. Silversmith and A. P. Radlinski, J. Phys. C **18**, 4385 (1985).
[12] A. P. Radlinski and A. J. Silversmith, Phys. Rev. B **34**, 86 (1986).
[13] D. Hommel and J. M. Langer, J. Lumin. **18/19**, 281 (1979).
[14] R. J. Hamers, J. R. Wietfeldt, and J. C. Wright, J. Chem. Phys. **77**, 683 (1982).
[15] J. P. Jouart, C. Bissieux, G. Mary, and M. Egee, J. Phys. C **18**, 1539 (1985).
[16] L. E. Erickson, Opt. Commun. **21**, 147 (1977).
[17] A. J. Silversmith and N. B. Manson, Phys. Rev. B **34**, 4854 (1986).